

Linear elastic mechanical system interacting with coupled thermo-electro-magnetic fields

Pablo Moreno-Navarro¹, Adnan Ibrahimbegovic^{*1} and José L. Pérez-Aparicio²

¹*Sorbonne Universités-Université de Technologie Compiègne, Laboratoire Roberval de Mécanique, Chaire de Mécanique, France*

²*Department of Continuum Mechanics & Theory of Structures, Universitat Politècnica de València, Spain*

(Received December 19, 2016, Revised February 20, 2017, Accepted May 26, 2017)

Abstract. A fully-coupled thermodynamic-based transient finite element formulation is proposed in this article for electric, magnetic, thermal and mechanic fields interactions limited to the linear case. The governing equations are obtained from conservation principles for both electric and magnetic flux, momentum and energy. A full-interaction among different fields is defined through Helmholtz free-energy potential, which provides that the constitutive equations for corresponding dual variables can be derived consistently. Although the behavior of the material is linear, the coupled interactions with the other fields are not considered limited to the linear case. The implementation is carried out in a research version of the research computer code FEAP by using 8-node isoparametric 3D solid elements. A range of numerical examples are run with the proposed element, from the relatively simple cases of piezoelectric, piezomagnetic, thermoelastic to more complicated combined coupled cases such as piezo-pyro-electric, or piezo-electro-magnetic. In this paper, some of those interactions are illustrated and discussed for a simple geometry.

Keywords: electromagnetic-thermomechanical coupling; elasticity; thermodynamics; finite element formulation

1. Introduction

Multi-coupled sensors and actuators are currently used in many state-of-the-art technological applications. The main interest of these materials does not reside in their strong primary interactions but in their secondary coupled interactions. In this paper, we are studying full-coupling of four different fields: thermal, electric, magnetic and mechanic.

Although the secondary coupled interactions are not as potent as the primary ones, with the proper conditioning can be suitable for sensing or triggering some circuits; for instance, by means of an electric amplifier or a relay. The main advantages of these materials are that their response is fast, trustworthy and, in a reasonable interval, linear. In addition, they can be inserted directly in a structure due to their reduced dimensions.

*Corresponding author, Professor, E-mail: adnan.ibrahimbegovic@utc.fr

This work seeks to provide a consistent thermodynamic development (Moreno-Navarro *et al.* 2017) for fully-coupled dielectric materials. First a set of state variables and their corresponding dual ones are defined for each field in establishing the governing equations based on conservation principles. Second, by settling a full quadratic form of the free-energy potential, the linear constitutive equations can be derived from it in a consistent way, providing a hyperelastic response instead of a hypoelastic. Finally, the theoretical formulation is accompanied by the discrete approximation, based upon 3D Finite Elements with thermo-electro-magneto-mechanic degrees of freedom, along with simultaneous solution procedures of the weak form for all governing equations.

In the literature there are numerous scientific articles on the coupling formulation of just two or three of the mentioned fields, such as piezoelectric (Allik and Hughes 1970), (Lezgy-Nazargah *et al.* 2013), (Safari and Akdogan 2008) and a special mention to (Duczek and Gabbert 2013) for the development of a piezoelectric element based on p-version finite element formulation first introduced in (Babuska *et al.* 1981); thermo-electro-elastic as in (Ryu *et al.* 2001), (Wang and Zhong 2003), (Ferrari and Mittica 2013); or electro-magneto-elastic as in (Ramirez *et al.* 2006), (Görnandt and Gabbert 2002), (Fung *et al.* 2000), (Rao and Sunar 1993), (Jiang and Li 2007), (Hou *et al.* 2006) and (Pan 2001). Others couple all fields but without a very consistent thermodynamic approach as in (Li 2000) or (Aboudi 2001). The recent ones that come closest to this work, not only because of their full-interaction approach but also for their thermodynamic framework are (Chen *et al.* 2004), (Pérez-Aparicio *et al.* 2015).

The outline of this paper is as follows. In Section 2, the theoretical formulation for thermo-electro-magnetic-mechanical coupling is presented first by giving all pertinent conservation principles and then by introducing the Helmholtz free-energy potential to obtain the constitutive equations for dual variables. The details for finite element implementation are given in Section 3 for 3D cases, using a discrete approximation constructed with isoparametric finite elements along with the time-integration Newmark scheme introduced in Section 4. Several numerical simulations are presented in Section 5, and the concluding remarks are given in Section 6.

2. Formulation

2.1 Kinematic equations

Four fields are considered in formulating the thermo-electro-magneto-mechanic coupling: displacement \mathbf{u} , temperature T , electric potential V and magnetic scalar potential φ . The state variables are obtained as the corresponding gradients of these fields. The set of resulting “kinematic” equations can be written as

$$\begin{aligned}\boldsymbol{\varepsilon} &= \frac{1}{2} [\nabla \otimes \mathbf{u} + (\nabla \otimes \mathbf{u})^T] \\ \mathbf{E} &= -\nabla V \\ \mathbf{H} &= -\nabla \varphi\end{aligned}\tag{1}$$

where $\boldsymbol{\varepsilon}$ is the strain tensor, \mathbf{E} is the electric field, \mathbf{H} is the magnetic field, while a convenient notation for the nabla operator of partial derivatives $\nabla = [\partial/\partial x \quad \partial/\partial y \quad \partial/\partial z]^T$ is used. With the hypothesis of small displacement gradient theory, we are limited here to strains defined in terms of the symmetric part of displacement gradient. Hence, the operator ∇^s can be used to define the

strain tensor, which can be written in Voigt notation as

$$\boldsymbol{\varepsilon} = \nabla^s \mathbf{u} ; \quad \nabla^s = \begin{bmatrix} \frac{\partial}{\partial x} & 0 & 0 \\ 0 & \frac{\partial}{\partial y} & 0 \\ 0 & 0 & \frac{\partial}{\partial z} \\ \frac{\partial}{\partial y} & \frac{\partial}{\partial x} & 0 \\ 0 & \frac{\partial}{\partial z} & \frac{\partial}{\partial y} \\ \frac{\partial}{\partial z} & 0 & \frac{\partial}{\partial x} \end{bmatrix} \quad (2)$$

2.2 Conservation principles

2.2.1 Conservation of electric and magnetic flux

The conservation of electric flux is given by the Gauss Law for electric field pertaining to a closed Gaussian surface, written by the following integral relationship

$$\Phi_e = \oiint_{\Gamma} \mathbf{E} \cdot d\boldsymbol{\Gamma} = \frac{Q}{\epsilon_0} \quad (3)$$

Here, Φ_e is the electric flux given by the closed surface integral of the electric field and the differential surface vector (normal to the outer surface Γ) scalar product. The flux is also equal to the total electric charge Q inside this surface divided by the vacuum (denoted by 0 subscript) permittivity ϵ_0 .

It is possible to obtain the equivalent differential expression from (3) by applying the divergence theorem to the closed surface integral, and by identifying $Q = \iiint_{\Omega} \rho_q \, d\Omega$ with ρ_q , the electric charge density

$$\nabla \cdot \mathbf{E} = \frac{\rho_q}{\epsilon_0} \quad (4)$$

In the absence of other fields and by taking into account the constitutive relation between \mathbf{E} and the electric displacement $\mathbf{D} = \epsilon_0 \mathbf{E} + \mathbf{P}$ (\mathbf{P} is the polarization), it is possible to rewrite the result in (4) in terms of \mathbf{D} , which is more suitable for macroscopic description

$$\nabla \cdot (\mathbf{D} - \mathbf{P}) = \rho_q \quad (5)$$

Finally, the decomposition $\rho_q = \rho_q^f + \rho_q^b$ into free and bound terms is introduced; the free term is associated with the movements of electrons in a conductor material and the bound term is related to the orientation of dipoles in a dielectric. By bringing in now the relation $\nabla \cdot \mathbf{P} = -\rho_q^b$, the result in (5) can be recast as

$$\nabla \cdot \mathbf{D} = \rho_q^f \quad (6)$$

An analogous expression can be found for the magnetic flux in terms of the Gauss Law for magnetism

$$\Phi_h = \oiint_{\Gamma} \mathbf{B} \cdot d\mathbf{\Gamma} = 0 \quad (7)$$

where Φ_h is the magnetic flux, given by the closed surface integral of the scalar product of the magnetic induction \mathbf{B} with the differential surface vector, that is equal to 0 stating the non-existence of magnetic monopoles. The local form of (7) can be obtained as the differential expression

$$\nabla \cdot \mathbf{B} = 0 \quad (8)$$

Both Eqs. (6) and (8) belong to Maxwell's equations in terms of the set of partial differential equations that fully define the electromagnetic behavior. These equations can be written in differential form (e.g., Balanis 1989) as follows

$$\begin{cases} \nabla \times \mathbf{E} = -\dot{\mathbf{B}} \\ \nabla \times \mathbf{H} = \mathbf{j} + \dot{\mathbf{D}} \\ \nabla \cdot \mathbf{D} = \rho_q^f \\ \nabla \cdot \mathbf{B} = 0 \end{cases} \quad (9)$$

where \mathbf{j} is the free electric charge flux. Since the targeted applications are dielectric materials, it can be assumed from here on that $\mathbf{j} = \mathbf{0}$ and $\rho_q^f = 0$ due to the absence of free electric charges (Balanis 1989).

2.2.2 Conservation of momentum

The classical approach to conservation of momentum (e.g., Ibrahimbegovic 2009) is now generalized to account for the electromagnetic field. First, by enforcing the angular momentum conservation we obtain the symmetry of stress tensor (e.g., Ibrahimbegovic 2009). Second, by postulating the linear momentum conservation principle for a domain, and in the limit case of the domain shrinking to a point, we obtain the local form of momentum conservation equation (de Groot and Mazur 1984)

$$\underbrace{\rho_m \ddot{\mathbf{u}}}_{\dot{\mathbf{p}}_m} + \underbrace{\frac{\dot{\mathbf{S}}}{c^2}}_{\dot{\mathbf{p}}_{eh}} = (\boldsymbol{\sigma}^C + \boldsymbol{\sigma}^M) \nabla + \mathbf{b} \quad (10)$$

where ρ_m is the mass density, \mathbf{p}_m the mechanical linear momentum, $\mathbf{S} = \mathbf{E} \times \mathbf{H}$ the Poynting vector, \mathbf{p}_{eh} the electromagnetic linear momentum, $\boldsymbol{\sigma}^C$ the Cauchy stress tensor, $\boldsymbol{\sigma}^M$ the Maxwell electromagnetic stress tensor, \mathbf{b} the volume forces and c the speed of light, related to the permeability and permittivity of the vacuum through the following expression

$$c^2 = \frac{1}{\epsilon_0 \mu_0} \quad (11)$$

This expression can be changed to transform the Maxwell stress tensor and the electromagnetic

linear momentum into a single corresponding force. With the definition of the dielectric constitutive relations for electromagnetic field

$$\begin{aligned} \mathbf{D} &= \epsilon_0 \mathbf{E} + \mathbf{P} = (\epsilon_0 \mathbf{I} + \chi_e) \mathbf{E} = \boldsymbol{\epsilon} \mathbf{E} \\ \mathbf{B} &= \mu_0 (\mathbf{H} + \mathbf{M}) = \mu_0 (\mathbf{I} + \chi_h) \mathbf{H} = \boldsymbol{\mu} \mathbf{H} \end{aligned} \quad (12)$$

with \mathbf{I} being unit second order tensor, χ_e , χ_h the electric and magnetic susceptibilities, $\boldsymbol{\epsilon}$ the permittivity tensor and $\boldsymbol{\mu}$ the permeability tensor. For dielectric materials, the polarization \mathbf{P} and the magnetization \mathbf{M} are proportional to \mathbf{E} and \mathbf{H} , respectively. Taking into account the last expression, the time derivative of the electromagnetic momentum (10) can be expanded into

$$\epsilon_0 \mu_0 \frac{\partial (\mathbf{E} \times \mathbf{H})}{\partial t} = \frac{\partial (\mathbf{D} \times \mathbf{B})}{\partial t} - \epsilon_0 \mu_0 \frac{\partial (\mathbf{E} \times \mathbf{M})}{\partial t} - \frac{\partial (\mathbf{P} \times \mathbf{B})}{\partial t} \quad (13)$$

By using the Maxwell's Eq. (9) and the following identity

$$(\nabla \times \mathbf{u}) \times \mathbf{v} = [\mathbf{v} \otimes \mathbf{u} - (\mathbf{u} \cdot \mathbf{v}) \mathbf{I}] \nabla - \mathbf{u} (\nabla \cdot \mathbf{v}) + (\nabla \otimes \mathbf{v}) \mathbf{u} \quad (14)$$

it is possible to obtain an alternative expression for the first term of the right-hand side

$$\frac{\partial (\mathbf{D} \times \mathbf{B})}{\partial t} = [\mathbf{D} \otimes \mathbf{E} + \mathbf{B} \otimes \mathbf{H} - (\mathbf{D} \cdot \mathbf{E} + \mathbf{B} \cdot \mathbf{H}) \mathbf{I}] \nabla + (\nabla \otimes \mathbf{D}) \mathbf{E} + (\nabla \otimes \mathbf{B}) \mathbf{H} \quad (15)$$

The last equation can also be transformed by using the following

$$\begin{aligned} (\nabla \otimes \mathbf{D}) \mathbf{E} &= \left[\left(\mathbf{P} \cdot \mathbf{E} + \frac{1}{2} \epsilon_0 \mathbf{E} \cdot \mathbf{E} \right) \mathbf{I} \right] \nabla - (\nabla \otimes \mathbf{E}) \mathbf{P} \\ (\nabla \otimes \mathbf{B}) \mathbf{H} &= \left[\frac{1}{2} \mu_0 (\mathbf{B} \cdot \mathbf{B}) \mathbf{I} \right] \nabla - (\nabla \otimes \mathbf{B}) \mathbf{M} \end{aligned} \quad (16)$$

By introducing all these identities into Eq. (15), we can write

$$\begin{aligned} \frac{\partial (\mathbf{D} \times \mathbf{B})}{\partial t} &= \left[\mathbf{D} \otimes \mathbf{E} + \mathbf{B} \otimes \mathbf{H} - \frac{\mathbf{I}}{2} (\epsilon_0 \mathbf{E} \cdot \mathbf{E} + \mu_0 \mathbf{B} \cdot \mathbf{B} - 2\mathbf{B} \cdot \mathbf{M}) \right] \nabla \\ &\quad - (\nabla \otimes \mathbf{E}) \mathbf{P} - (\nabla \otimes \mathbf{B}) \mathbf{M} \end{aligned} \quad (17)$$

With these results at hand, we return to Eq. (13), with three terms set apart

$$\dot{\mathbf{p}}_{\text{eh}} = \boldsymbol{\sigma}^M \nabla + \mathbf{b}_{\text{eh}} \quad (18)$$

where by identification

$$\begin{cases} \mathbf{b}_{\text{eh}} := -(\nabla \otimes \mathbf{E}) \mathbf{P} - (\nabla \otimes \mathbf{B}) \mathbf{M} - \epsilon_0 \mu_0 \frac{\partial (\mathbf{E} \times \mathbf{M})}{\partial t} - \frac{\partial (\mathbf{P} \times \mathbf{B})}{\partial t} \\ \boldsymbol{\sigma}^M := \mathbf{D} \otimes \mathbf{E} + \mathbf{B} \otimes \mathbf{H} - \frac{\mathbf{I}}{2} (\epsilon_0 \mathbf{E} \cdot \mathbf{E} + \mu_0 \mathbf{B} \cdot \mathbf{B} - 2\mathbf{B} \cdot \mathbf{M}) \end{cases} \quad (19)$$

The electromagnetic force \mathbf{b}_{eh} , which accounts for the distributed electric and magnetic force that can arise due to the possible presence of a non-uniform electrical or magnetic field in the material (Ferrari and Mittica 2013). Finally, the conservation of momentum (10) can be expressed in terms of \mathbf{b}_{eh} simply as

$$\rho_m \ddot{\mathbf{u}} = \boldsymbol{\sigma} \nabla + \mathbf{b}_{\text{eh}} + \mathbf{b} \quad (20)$$

where the Cauchy superscript C has been drop from $\boldsymbol{\sigma}$ for simplicity.

2.2.3 Conservation of energy

The global form of the first principle of thermodynamics can be stated in a closed domain Ω

$$\frac{\partial}{\partial t} E = W_m + W_{eh} + Q \quad (21)$$

where E is the total energy, W_m is the mechanical power, W_{eh} is the electromagnetic power and Q is the total heat supplied to that domain. The total energy can be split into potential P and kinetic K energy terms

$$E = P + K = \int_{\Omega} \mathbf{e}(\boldsymbol{\varepsilon}, s, \mathbf{D}, \mathbf{B}) \, d\Omega + \frac{1}{2} \int_{\Omega} \rho_m \dot{\mathbf{u}} \cdot \dot{\mathbf{u}} \, d\Omega \quad (22)$$

where e is the scalar potential of the internal energy density that depends on the state variables. The list of state variables is defined in Table 1, along with their corresponding dual variables (with s as the entropy per unit volume).

Table 1 List of the state variables and their corresponding dual variables for coupled thermoelasticity and electromagnetism

Fields	Mechanic	Thermal	Electric	Magnetic
State variable	$\boldsymbol{\varepsilon}$	s	\mathbf{D}	\mathbf{B}
Dual variable	$\boldsymbol{\sigma}$	T	\mathbf{E}	\mathbf{H}

The source of mechanical power inserted within the particular domain Ω can be written as

$$W_m := \int_{\Omega} (\mathbf{b} + \mathbf{b}_{eh}) \cdot \dot{\mathbf{u}} \, d\Omega + \int_{\Gamma} \mathbf{t}^n \cdot \dot{\mathbf{u}} \, d\Gamma = \int_{\Omega} (\mathbf{b} + \mathbf{b}_{eh}) \cdot \dot{\mathbf{u}} \, d\Omega + \int_{\Omega} \nabla \cdot (\boldsymbol{\sigma} \dot{\mathbf{u}}) \, d\Omega \quad (23)$$

where \mathbf{n} is unit normal vector. The last term is defined from the boundary traction vector \mathbf{t}^n by the Cauchy principle $\mathbf{t}^n = \boldsymbol{\sigma} \mathbf{n}$; this vector has been transformed into the corresponding volume integral with the divergence theorem. A similar integral transformation can be done for the boundary term of the electromagnetic power source (see Balanis 1989), and it is defined as

$$W_{eh} := - \int_{\Gamma} (\mathbf{E} \times \mathbf{H}) \cdot \mathbf{n} \, d\Gamma = - \int_{\Omega} \nabla \cdot (\mathbf{E} \times \mathbf{H}) \, d\Omega \quad (24)$$

We note in passing that the negative sign is in agreement with the above expression representation of total power exiting the volume Ω bounded by the surface Γ . Similar transformation can finally be made for the heat power source that stems from the outgoing heat flux \mathbf{q} , along with the heat source r , which results in

$$Q := \int_{\Omega} r \, d\Omega - \int_{\Gamma} \mathbf{q} \cdot \mathbf{n} \, d\Gamma = \int_{\Omega} r \, d\Omega - \int_{\Omega} \nabla \cdot \mathbf{q} \, d\Omega \quad (25)$$

In the limit case of Ω shrinking to a point, we obtain from (21) the local form of the first

principle, which can be written as

$$\dot{\epsilon}(\epsilon, s, \mathbf{D}, \mathbf{B}) + \rho_m \ddot{\mathbf{u}} \cdot \dot{\mathbf{u}} = (\mathbf{b} + \mathbf{b}_{\text{eh}}) \cdot \dot{\mathbf{u}} + \nabla \cdot (\boldsymbol{\sigma} \dot{\mathbf{u}}) + r - \nabla \cdot \mathbf{q} - \nabla \cdot (\mathbf{E} \times \mathbf{H}) \quad (26)$$

Furthermore, by substituting the kinematic equations in (1) and the equation of motion in (20), along with the identity $\nabla \cdot (\boldsymbol{\sigma} \dot{\mathbf{u}}) = (\boldsymbol{\sigma} \nabla) \cdot \dot{\mathbf{u}} + \boldsymbol{\sigma} \cdot (\nabla \otimes \dot{\mathbf{u}})$, we can obtain the reduced form of the first principle or energy conservation

$$\dot{\epsilon}(\epsilon, s, \mathbf{D}, \mathbf{B}) = \boldsymbol{\sigma} \cdot \dot{\epsilon} + r - \nabla \cdot \mathbf{q} - \nabla \cdot (\mathbf{E} \times \mathbf{H}) \quad (27)$$

The final ingredient left is to provide the definition of the heat flux through Fourier's law

$$\mathbf{q} = -\kappa \nabla T \quad (28)$$

where κ is the thermal conductivity.

By scalar multiplication of the first two Maxwell's equations of (9) with \mathbf{H} and \mathbf{E} respectively, and by exploiting the following identity

$$\nabla \cdot (\mathbf{E} \times \mathbf{H}) = \mathbf{H} \cdot (\nabla \times \mathbf{E}) - \mathbf{E} \cdot (\nabla \times \mathbf{H}) \quad (29)$$

the reduced form of energy conservation (27) can be recast in an equivalent format

$$\dot{\epsilon}(\epsilon, s, \mathbf{D}, \mathbf{B}) = \boldsymbol{\sigma} \cdot \dot{\epsilon} + r - \nabla \cdot \mathbf{q} + \mathbf{E} \cdot \dot{\mathbf{D}} + \mathbf{H} \cdot \dot{\mathbf{B}} \quad (30)$$

The second principle of thermodynamics imposes that the rate of increase of entropy \dot{S} should never be smaller than the amount of heat divided by the absolute temperature. For a particular domain Ω we can write

$$\dot{S} \geq \frac{\mathbf{Q}}{T}; \quad S = \int_{\Omega} s \, d\Omega \quad (31)$$

In the limit case of shrinking the domain to a point, we can obtain the local form of the second principle. In the simplest case of a rigid conductor (corresponds to neglecting all fields but the thermal), the second principle provides the proper definition of dissipation by conduction \mathcal{D}^c (Ibrahimbegovic 2009), which always remains positive as long as Fourier's law applies

$$-\underbrace{\frac{1}{T} \mathbf{q} \cdot \nabla T}_{\mathcal{D}^c} := T \dot{s} - (r - \nabla \cdot \mathbf{q}) \geq 0 \quad (32)$$

The second principle, combined with the result of the first principle in (30) can be used to define the local dissipation, which always remains non-negative

$$\mathcal{D} := T \dot{s} - \dot{\epsilon}(\epsilon, s, \mathbf{D}, \mathbf{B}) + \boldsymbol{\sigma} \cdot \dot{\epsilon} + \mathbf{E} \cdot \dot{\mathbf{D}} + \mathbf{H} \cdot \dot{\mathbf{B}} \geq 0 \quad (33)$$

In the result above we dropped the dissipation by conduction. We can introduce the free energy potential by appealing to the Legendre transformation (e.g., Ibrahimbegovic 2009), which allows to exchange the roles between the state variables and their dual, $s, \mathbf{D}, \mathbf{B}$ versus $T, \mathbf{E}, \mathbf{H}$

$$\psi(\epsilon, T, \mathbf{E}, \mathbf{H}) = \mathbf{e}(\epsilon, s, \mathbf{D}, \mathbf{B}) - T s - \mathbf{E} \cdot \mathbf{D} - \mathbf{H} \cdot \mathbf{B} \quad (34)$$

Deriving with respect to time the last expression we can obtain

$$\dot{\varepsilon} = \frac{\partial \psi}{\partial \varepsilon} \cdot \dot{\varepsilon} + \frac{\partial \psi}{\partial T} \dot{T} + \frac{\partial \psi}{\partial \mathbf{E}} \cdot \dot{\mathbf{E}} + \frac{\partial \psi}{\partial \mathbf{H}} \cdot \dot{\mathbf{H}} + \dot{T} s + T \dot{s} + \mathbf{E} \cdot \dot{\mathbf{D}} + \dot{\mathbf{E}} \cdot \mathbf{D} + \mathbf{H} \cdot \dot{\mathbf{B}} + \dot{\mathbf{H}} \cdot \mathbf{B} \quad (35)$$

With this result on hand, the dissipation (33) can be expressed as

$$0 \leq \mathcal{D} = \left(\boldsymbol{\sigma} - \frac{\partial \psi}{\partial \varepsilon} \right) \cdot \dot{\varepsilon} - \left(s + \frac{\partial \psi}{\partial T} \right) \dot{T} - \left(\mathbf{D} + \frac{\partial \psi}{\partial \mathbf{E}} \right) \cdot \dot{\mathbf{E}} - \left(\mathbf{B} + \frac{\partial \psi}{\partial \mathbf{H}} \right) \cdot \dot{\mathbf{H}} \quad (36)$$

The dissipation inequality will become an equality providing the set of constitutive equations to be defined in agreement with the chosen free energy potential. Here, we choose a quadratic form of the free energy potential, which can be written as follows

$$\psi(\varepsilon^e, \zeta, T, \mathbf{E}, \mathbf{H}) = \psi_m + \psi_t + \psi_e + \psi_h + \psi_{mt} + \psi_{me} + \psi_{mh} + \psi_{te} + \psi_{th} + \psi_{eh};$$

$$\begin{aligned} \psi_m &= \frac{1}{2} \varepsilon \cdot \mathbf{C} \varepsilon; & \psi_{me} &= -\varepsilon \cdot \mathbf{e}_e \mathbf{E}; \\ \psi_t &= \rho_m c_v \left[(T - T_0) - T \ln \frac{T}{T_0} \right]; & \psi_{mh} &= -\varepsilon \cdot \mathbf{e}_h \mathbf{H}; \\ \psi_e &= -\frac{1}{2} \mathbf{E} \cdot \boldsymbol{\epsilon} \mathbf{E}; & \psi_{te} &= -(T - T_0) \boldsymbol{\pi}_e \cdot \mathbf{E}; \\ \psi_h &= -\frac{1}{2} \mathbf{H} \cdot \boldsymbol{\mu} \mathbf{H}; & \psi_{th} &= -(T - T_0) \boldsymbol{\pi}_h \cdot \mathbf{H}; \\ \psi_{mt} &= -(T - T_0) \boldsymbol{\beta} \cdot \varepsilon; & \psi_{eh} &= -\mathbf{E} \cdot \boldsymbol{\nu} \mathbf{H} \end{aligned} \quad (37)$$

where \mathbf{C} is the elasticity tensor, c_v the specific heat, $\boldsymbol{\beta} = \mathbf{C} \alpha_T \mathbf{I}$ the thermal isotropic stress tensor (with α_T as the expansion coefficient), \mathbf{e}_e the piezoelectric tensor, \mathbf{e}_h the piezomagnetic tensor, $\boldsymbol{\pi}_e$ the pyroelectric vector, $\boldsymbol{\pi}_h$ the piezomagnetic vector and $\boldsymbol{\nu}$ the magnetoelectric tensor. The corresponding hyperelastic constitutive equations can easily be obtained by derivatives of such a potential with respect to the state variables

$$\begin{cases} \boldsymbol{\sigma} := \frac{\partial \psi}{\partial \varepsilon} = \mathbf{C} \varepsilon - \boldsymbol{\beta} (T - T_0) - \mathbf{e}_e \mathbf{E} - \mathbf{e}_h \mathbf{H} \\ s := -\frac{\partial \psi}{\partial T} = \boldsymbol{\beta} \cdot \varepsilon + \rho_m c_v \ln \left(\frac{T}{T_0} \right) + \boldsymbol{\pi}_e \cdot \mathbf{E} + \boldsymbol{\pi}_h \cdot \mathbf{H} \\ \mathbf{D} := -\frac{\partial \psi}{\partial \mathbf{E}} = \mathbf{e}_e \varepsilon + \boldsymbol{\pi}_e (T - T_0) + \boldsymbol{\epsilon} \mathbf{E} + \boldsymbol{\nu} \mathbf{H} \\ \mathbf{B} := -\frac{\partial \psi}{\partial \mathbf{H}} = \mathbf{e}_h \varepsilon + \boldsymbol{\pi}_h (T - T_0) + \boldsymbol{\nu} \mathbf{E} + \boldsymbol{\mu} \mathbf{H} \end{cases} \quad (38)$$

Again, with these results on hand, we can write from (32) the heat equation for an elastic case as

$$T \dot{s} = r - \nabla \cdot \mathbf{q} \quad (39)$$

where all terms in the expression for dissipation (36) are zero due to the constitutive equation definitions. Furthermore, by using the entropy s from (38), we can rewrite the heat equation

$$\rho_m c_v \dot{T} = r - \nabla \cdot \mathbf{q} - T \left(\boldsymbol{\beta} \cdot \dot{\varepsilon} + \boldsymbol{\pi}_e \cdot \dot{\mathbf{E}} + \boldsymbol{\pi}_h \cdot \dot{\mathbf{H}} \right) \quad (40)$$

In summary, the strong form of the balance equations regroups the results written in (6), (8), (20) and (40), here restated in tensor notation

$$\left\{ \begin{array}{l} \rho_m \ddot{\mathbf{u}} = \boldsymbol{\sigma} \nabla + \mathbf{b}_{\text{eh}} + \mathbf{b} \\ \nabla \cdot \mathbf{D} = 0 \\ \nabla \cdot \mathbf{B} = 0 \\ \rho_m c_v \dot{T} = r - \nabla \cdot \mathbf{q} - T \left(\boldsymbol{\beta} \cdot \dot{\boldsymbol{\varepsilon}} + \boldsymbol{\pi}_e \cdot \dot{\mathbf{E}} + \boldsymbol{\pi}_h \cdot \dot{\mathbf{H}} \right) \end{array} \right. \quad (41)$$

3. Finite element implementation

In this section, we present the details of the discrete approximation constructed by the finite element method, as a particular case of the Galerkin method. The starting point is provided by the weak form of the conservation equations, which can be stated in tensor notation as follows

$$\left\{ \begin{array}{l} - \int_{\Omega} \nabla^s \delta \mathbf{u} \cdot \boldsymbol{\sigma} + \delta \mathbf{u} \cdot (\rho_m \ddot{\mathbf{u}} - \mathbf{b}_{\text{eh}} - \mathbf{b}) \, d\Omega + \int_{\Gamma} \delta \mathbf{u} \cdot \bar{\mathbf{t}}^c \, d\Gamma = 0 ; \\ \int_{\Omega} \nabla \delta V \cdot \mathbf{D} \, d\Omega - \int_{\Gamma} \delta V \bar{D} \, d\Gamma = 0 ; \\ \int_{\Omega} \nabla \delta \varphi \cdot \mathbf{B} \, d\Omega - \int_{\Gamma} \delta \varphi \bar{B} \, d\Gamma = 0 ; \\ \int_{\Omega} \nabla \delta T \cdot \mathbf{q} - \delta T \left[\rho_m c_v \dot{T} - r + T \left(\boldsymbol{\beta} \cdot \dot{\boldsymbol{\varepsilon}} + \boldsymbol{\pi}_e \cdot \dot{\mathbf{E}} + \boldsymbol{\pi}_h \cdot \dot{\mathbf{H}} \right) \right] \, d\Omega \\ - \int_{\Gamma} \delta T \bar{q} \, d\Gamma = 0 \end{array} \right. \quad (42)$$

The overbar denotes prescribed magnitudes. We can readily obtain the discrete approximations for all the fields (Ibrahimbegovic 2009), along with their space and time derivatives by appealing to separation of variables in Einstein summation convention

$$\begin{array}{llll} \mathbf{u} \approx \mathcal{N}_b \mathbf{a}_b^U ; & V \approx \mathcal{N}_b a_b^V ; & \varphi \approx \mathcal{N}_b a_b^\varphi ; & T \approx \mathcal{N}_b a_b^T ; \\ \delta \mathbf{u} \approx \mathcal{N}_a \mathbf{w}_a^U ; & \delta V \approx \mathcal{N}_a w_a^V ; & \delta \varphi \approx \mathcal{N}_a w_a^\varphi ; & \delta T \approx \mathcal{N}_a w_a^T ; \\ \nabla^s \mathbf{u} \approx \mathcal{B}_b^s \mathbf{a}_b^U ; & \nabla V \approx \mathcal{B}_b a_b^V ; & \nabla \varphi \approx \mathcal{B}_b a_b^\varphi ; & \nabla T \approx \mathcal{B}_b a_b^T ; \\ \nabla^s \delta \mathbf{u} \approx \mathcal{B}_a^s \mathbf{w}_a^U ; & \nabla \delta V \approx \mathcal{B}_a w_a^V ; & \nabla \delta \varphi \approx \mathcal{B}_a w_a^\varphi ; & \nabla \delta T \approx \mathcal{B}_a w_a^T ; \\ \nabla^s \dot{\mathbf{u}} \approx \mathcal{B}_b^s \dot{\mathbf{a}}_b^U ; & \nabla \dot{V} \approx \mathcal{B}_b \dot{a}_b^V ; & \nabla \dot{\varphi} \approx \mathcal{B}_b \dot{a}_b^\varphi ; & \dot{T} \approx \mathcal{N}_b \dot{a}_b^T ; \\ \ddot{\mathbf{u}} \approx \mathcal{N}_b \ddot{\mathbf{a}}_b^U ; & a = 1, 2, \dots, 8 & b = 1, 2, \dots, 8 \end{array} \quad (43)$$

where \mathbf{a} represents the nodal values of different fields (often called degrees of freedom), whereas \mathbf{w} represents the nodal values of their variations or virtual nodal degrees of freedom. In the last expression, \mathcal{N}_a denotes the standard isoparametric shape function for node a (e.g. Ibrahimbegovic 2009). The subscript a and b respond to the need of splitting the shape functions associated with virtual nodal values and real nodal values for posterior summations. The gradients of the shape functions are gathered in convenient forms as

$$\begin{array}{l} \mathcal{B}_a = \nabla \mathcal{N}_a ; \\ \mathcal{B}_a^s = \nabla^s \mathcal{N}_a \end{array} \quad (44)$$

By introducing the corresponding finite element approximations into the weak form of the conservation equations, and by changing from tensors to matrices by means of the Voigt notation, we can finally obtain

$$\left\{ \begin{array}{l} - \int_{\Omega} (\mathbf{B}_a^s \mathbf{w}_a^U)^\top \boldsymbol{\sigma} + (\mathcal{N}_a \mathbf{w}_a^U)^\top (\rho_m \mathcal{N}_b \ddot{\mathbf{a}}_b^U - \mathbf{b}_{\text{eh}} - \mathbf{b}) \, d\Omega + \int_{\Gamma} (\mathcal{N}_a \mathbf{w}_a^U)^\top \bar{\mathbf{t}}^c \, d\Gamma = 0 ; \\ \int_{\Omega} (\mathbf{B}_a \mathbf{w}_a^V)^\top \mathbf{D} \, d\Omega - \int_{\Gamma} \mathcal{N}_a \mathbf{w}_a^V \bar{D} \, d\Gamma = 0 ; \\ \int_{\Omega} (\mathbf{B}_a \mathbf{w}_a^\varphi)^\top \mathbf{B} \, d\Omega - \int_{\Gamma} \mathcal{N}_a \mathbf{w}_a^\varphi \bar{B} \, d\Gamma = 0 ; \\ \int_{\Omega} (\mathbf{B}_a \mathbf{w}_a^T)^\top \mathbf{q} - \mathcal{N}_a \mathbf{w}_a^T \left[\rho_m c_v \mathcal{N}_b \dot{\mathbf{a}}_b^T - r + \mathcal{N}_b \mathbf{a}_b^T \left(\beta^\top \mathbf{B}_b^s \dot{\mathbf{a}}_b^U - \pi_\epsilon^\top \mathbf{B}_b \dot{\mathbf{a}}_b^V \right. \right. \\ \left. \left. - \pi_h^\top \mathbf{B}_b \dot{\mathbf{a}}_b^\varphi \right) \right] \, d\Omega - \int_{\Gamma} \mathcal{N}_a \mathbf{w}_a^T \bar{q} \, d\Gamma = 0 \end{array} \right. \quad (45)$$

where we introduced the discrete approximations into the dual variables

$$\left\{ \begin{array}{l} \boldsymbol{\sigma} = \mathbf{C} \mathbf{B}_b^s \mathbf{a}_b^U - \beta (\mathcal{N}_b \mathbf{a}_b^T - T_0) + \mathbf{e}_\epsilon^\top \mathbf{B}_b \mathbf{a}_b^V + \mathbf{e}_h^\top \mathbf{B}_b \mathbf{a}_b^\varphi ; \\ \mathbf{D} = \mathbf{e}_\epsilon \mathbf{B}_b^s \mathbf{a}_b^U + \pi_\epsilon (\mathcal{N}_b \mathbf{a}_b^T - T_0) - \epsilon \mathbf{B}_b \mathbf{a}_b^V - \nu \mathbf{B}_b \mathbf{a}_b^\varphi ; \\ \mathbf{B} = \mathbf{e}_h \mathbf{B}_b^s \mathbf{a}_b^U + \pi_h (\mathcal{N}_b \mathbf{a}_b^T - T_0) - \nu \mathbf{B}_b \mathbf{a}_b^V - \mu \mathbf{B}_b \mathbf{a}_b^\varphi \end{array} \right. \quad (46)$$

By considering that the nodal values of virtual field $\forall \mathbf{w}$ can be picked up arbitrarily, it is possible to obtain from (45) the final set of residuals equations that need to be solved

$$\left\{ \begin{array}{l} \mathcal{R}_a^U = - \int_{\Omega} \mathbf{B}_a^s \boldsymbol{\sigma} + \mathcal{N}_a (\rho_m \mathcal{N}_b \ddot{\mathbf{a}}_b^U - \mathbf{b}_{\text{eh}} - \mathbf{b}) \, d\Omega + \int_{\Gamma} \mathcal{N}_a \bar{\mathbf{t}}^c \, d\Gamma ; \\ \mathcal{R}_a^V = \int_{\Omega} \mathbf{B}_a^\top \mathbf{D} \, d\Omega - \int_{\Gamma} \mathcal{N}_a \bar{D} \, d\Gamma ; \\ \mathcal{R}_a^\varphi = \int_{\Omega} \mathbf{B}_a^\top \mathbf{B} \, d\Omega - \int_{\Gamma} \mathcal{N}_a \bar{B} \, d\Gamma ; \\ \mathcal{R}_a^T = \int_{\Omega} \mathbf{B}_a^\top \mathbf{q} - \mathcal{N}_a \left[\rho_m c_v \mathcal{N}_b \dot{\mathbf{a}}_b^T - r + \mathcal{N}_b \mathbf{a}_b^T \left(\beta^\top \mathbf{B}_b^s \dot{\mathbf{a}}_b^U - \pi_\epsilon^\top \mathbf{B}_b \dot{\mathbf{a}}_b^V \right. \right. \\ \left. \left. - \pi_h^\top \mathbf{B}_b \dot{\mathbf{a}}_b^\varphi \right) \right] \, d\Omega - \int_{\Gamma} \mathcal{N}_a \bar{q} \, d\Gamma \end{array} \right. \quad (47)$$

4. Time discretization by Newmark scheme

The Newmark scheme is used for the time discretization of the global solution step. This scheme requires two parameters γ and β that will determine the numerical damping and order of the scheme (e.g., Ibrahimbegovic 2009)

$$\begin{aligned} \mathbf{a}_{b,n+1} &= \mathbf{a}_{b,n} + \Delta t \dot{\mathbf{a}}_{b,n} + \Delta t^2 \left[\left(\frac{1}{2} - \beta \right) \ddot{\mathbf{a}}_{b,n} + \beta \ddot{\mathbf{a}}_{b,n+1} \right] ; \\ \dot{\mathbf{a}}_{b,n+1} &= \dot{\mathbf{a}}_{b,n} + \Delta t [(1 - \gamma) \ddot{\mathbf{a}}_{b,n} + \gamma \ddot{\mathbf{a}}_{b,n+1}] \end{aligned} \quad (48)$$

where we denoted the time step as $\Delta t = t_{n+1} - t_n$. These expressions, often referred to as Newmark equations and are accompanied by the equation enforcing the zero value of the residuals at time step $n + 1$, which can be explicitly written as

$$\left\{ \begin{array}{l} \mathcal{R}_{a,n+1}^{U,(i)} = - \int_{\Omega} \mathbf{B}_a^{s\top} \boldsymbol{\sigma}_{n+1}^{(i)} + \mathcal{N}_a \left(\rho_m \mathcal{N}_b \ddot{\mathbf{a}}_{b,n+1}^{U,(i)} - \mathbf{b}_{\text{eh},n+1}^{(i)} - \mathbf{b}_{n+1} \right) d\Omega + \int_{\Gamma} \mathcal{N}_a \bar{t}_{n+1}^c d\Gamma ; \\ \mathcal{R}_{a,n+1}^{V,(i)} = \int_{\Omega} \mathbf{B}_a^{\top} \mathbf{D}_{n+1}^{(i)} d\Omega - \int_{\Gamma} \mathcal{N}_a \bar{D}_{n+1} d\Gamma ; \\ \mathcal{R}_{a,n+1}^{\varphi,(i)} = \int_{\Omega} \mathbf{B}_a^{\top} \mathbf{B}_{n+1}^{(i)} d\Omega - \int_{\Gamma} \mathcal{N}_a \bar{B}_{n+1} d\Gamma ; \\ \mathcal{R}_{a,n+1}^T = \int_{\Omega} \mathbf{B}_a^{\top} \mathbf{q}_{n+1}^{(i)} - \mathcal{N}_a \left[\rho_m c_v \mathcal{N}_b \dot{\mathbf{a}}_{b,n+1}^{T,(i)} - r_{n+1} + \mathcal{N}_b \mathbf{a}_{b,n+1}^{T,(i)} \left(\beta^{\top} \mathbf{B}_b^s \dot{\mathbf{a}}_{b,n+1}^{U,(i)} \right. \right. \\ \left. \left. - \pi_e^{\top} \mathbf{B}_b \dot{\mathbf{a}}_{b,n+1}^{V,(i)} - \pi_h^{\top} \mathbf{B}_b \dot{\mathbf{a}}_{b,n+1}^{\varphi,(i)} \right) \right] d\Omega - \int_{\Gamma} \mathcal{N}_a \bar{q}_{n+1} d\Gamma \end{array} \right. \quad (49)$$

Thus, this type of time stepping scheme will render the set of nonlinear algebraic equations. To solve such a nonlinear problem, we use Newton's iterative method where at each iteration ($i + 1$) we perform the consistent linearization of residuals leading to

$$\mathcal{R}_{a,n+1}^{(i+1)} = 0 \Rightarrow \mathcal{R}_{a,n+1}^{(i)} + \left. \frac{\partial \mathcal{R}_{a,n+1}}{\partial \mathbf{b}_{b,n+1}} \right|^{(i)} \delta \mathbf{b}_{b,n+1}^{(i)} = 0 ; \quad \mathcal{R}_{a,n+1}^{(i)} = [\mathcal{R}^U, \mathcal{R}^V, \mathcal{R}^{\varphi}, \mathcal{R}^T]_{a,n+1}^{\top,(i)} \quad (50)$$

where $\delta \mathbf{b}_b$ are iterative contributions to nodal values of the degrees of freedom and its time derivatives. In this case, we are using the displacement description $\mathbf{b} := \mathbf{a}$. At each iterative sweep, we can then perform the corresponding state variable updates according to

$$\mathbf{a}_{b,n+1}^{(i+1)} = \mathbf{a}_{b,n+1}^{(i)} + \delta \mathbf{a}_{b,n+1}^{(i)} \quad (51)$$

In the first iteration within each time step we will assume the starting guess equal to the converged value at the previous step

$$\mathbf{a}_{b,n+1}^{(0)} = \mathbf{a}_{b,n} \quad (52)$$

The mechanical part of the residual vector at particular iteration (i) can be compressed, reducing it to the form presented explicitly in (49). Namely, the derivative term in (50) can be reduced to so-called effective tangent stiffness for the mechanical part, which is directly used to compute the iterative contributions to the displacement increments

$$\mathbf{S}_{ab}^{U,(i)} = - \left. \frac{\partial \mathcal{R}_a^U}{\partial \mathbf{a}_b} \right|^{(i)} - \left. \frac{\partial \mathcal{R}_a^U}{\partial \dot{\mathbf{a}}_b} \frac{\partial \dot{\mathbf{a}}_b}{\partial \mathbf{a}_b} \right|^{(i)} - \left. \frac{\partial \mathcal{R}_a^U}{\partial \ddot{\mathbf{a}}_b} \frac{\partial \ddot{\mathbf{a}}_b}{\partial \mathbf{a}_b} \right|^{(i)} \quad (53)$$

where the time-step subscript $n + 1$ was dropped to simplify notation. By exploiting the relations between the nodal displacements and its first and second derivatives provided by the Newmark scheme, we can write the closed form final linearized problem to be solved. More precisely, in view of the Newmark result for constructing discrete approximations for nodal velocities and accelerations in (48), we can write

$$\frac{\partial \ddot{\mathbf{a}}_b}{\partial \mathbf{a}_b} = \frac{1}{\beta \Delta t^2} ; \quad \frac{\partial \dot{\mathbf{a}}_b}{\partial \mathbf{a}_b} = \frac{\partial \dot{\mathbf{a}}_b}{\partial \ddot{\mathbf{a}}_b} \frac{\partial \ddot{\mathbf{a}}_b}{\partial \mathbf{a}_b} = \frac{\gamma}{\beta \Delta t} \quad (54)$$

Thus, the final form of the tangent operator for the mechanical part can now be written as

$$\mathcal{S}_{ab}^{U,(i)} = \mathcal{K}_{ab}^{(i)} + \frac{\gamma}{\beta \Delta t} \mathcal{C}_{ab} + \frac{1}{\beta \Delta t^2} \mathcal{M}_{ab} \quad (55)$$

where $\mathcal{K}_{ab}^{(i)} = -\frac{\partial \mathcal{R}_a}{\partial \mathbf{a}_b}$ is the tangent stiffness matrix, $\mathcal{C}_{ab} = -\frac{\partial \mathcal{R}_a}{\partial \dot{\mathbf{a}}_b}$ is the damping matrix and $\mathcal{M}_{ab} = -\frac{\partial \mathcal{R}_a}{\partial \ddot{\mathbf{a}}_b}$ is the mass matrix.

Given the solution for displacement increment at iteration (i), we proceed to compute the displacement updates $\mathbf{a}_{n+1}^{(i+1)}$ by using the result in (51). The corresponding values for $\dot{\mathbf{a}}_{n+1}^{(i+1)}$ and $\ddot{\mathbf{a}}_{n+1}^{(i+1)}$ are obtained by isolating $\ddot{\mathbf{a}}_{n+1}^{(i+1)}$ from the first of (48), and $\dot{\mathbf{a}}_{n+1}^{(i+1)}$ directly from the second, resulting with

$$\begin{aligned} \ddot{\mathbf{a}}_{b,n+1}^{(i+1)} &= \frac{\mathbf{a}_{b,n+1}^{(i+1)} - \mathbf{a}_{b,n} - \Delta t \dot{\mathbf{a}}_{b,n}}{\beta \Delta t^2} + \left(1 - \frac{1}{2\beta}\right) \ddot{\mathbf{a}}_{b,n}; \\ \dot{\mathbf{a}}_{b,n+1}^{(i+1)} &= \dot{\mathbf{a}}_{b,n} + \Delta t \left[(1 - \gamma) \ddot{\mathbf{a}}_{b,n} + \gamma \ddot{\mathbf{a}}_{b,n+1}^{(i+1)} \right] \end{aligned} \quad (56)$$

5. Numerical examples

In this section, several applications are studied as examples of the constructed element capabilities. All computations are performed in a research version of the well-known computer code FEAP (Zienkiewicz and Taylor 2005).

The polarized and magnetized materials have a preferential direction due to their internal structure (Smith 2005). As a result, a transverse isotropic model is taken into consideration, model that leads into vectors for $\boldsymbol{\pi}_e$ and $\boldsymbol{\pi}_h$, diagonal tensors for $\boldsymbol{\mu}$, $\boldsymbol{\epsilon}$, $\boldsymbol{\nu}$ and $\boldsymbol{\beta}$, the last four with a component different than the others (the polarized direction). For the remaining coefficients, a simplification from a full form tensor into a symmetric one with many null entries is necessary; the non-zero coefficients are related among them. All strain related coefficients are expressed in what follows in Voigt notation: $\boldsymbol{\beta}$, \mathbf{e}_e , \mathbf{e}_h , \mathbf{C} .

Introducing the notation of a second order diagonal tensor

$$\text{diag}(a_1, a_2, a_3) = \begin{bmatrix} a_1 & 0 & 0 \\ 0 & a_2 & 0 \\ 0 & 0 & a_3 \end{bmatrix} \quad (57)$$

unless otherwise said, the properties extracted from (Ferrari and Mittica 2013), (Ramirez *et al.* 2006) and (Pérez-Aparicio *et al.* 2015) for the materials studied in this section are presented in (58). These properties correspond to different materials: PZT, Terfenol-D, BaTiO₃ or CoFe₂O₄; however, in this paper, they artificially belong to the same material just for calculation purposes.

$$\begin{aligned} \rho_m &= 5700 \text{ kg/m}^3 & c_v &= 434 \text{ J/kg K} \\ \kappa &= 2.61 \text{ W/m K} & T_0 &= 293 \text{ K} \\ \epsilon &= \text{diag}(11.2, 11.2, 12.6) \times 10^{-9} \text{ F/m} & \mu &= \text{diag}(5, 5, 10) \times 10^{-6} \text{ H/m} \\ \nu &= \text{diag}(5.37, 5.37, 2737.5) \times 10^{-12} \text{ s/m} & \beta &= [1.67, 1.67, 1.96, 0, 0, 0]^T \text{ MPa/K} \\ \boldsymbol{\pi}_e &= [58.3, 58.3, 58.3]^T \times 10^{-5} \text{ C/m}^2 \text{ K} & \boldsymbol{\pi}_h &= [5, 5, 5]^T \times 10^{-2} \text{ kg/s}^2 \text{ A K} \end{aligned}$$

$$\mathbf{e}_e = \begin{bmatrix} 0 & 0 & 0 & 0 & 0 & 0 & 11.6 \\ 0 & 0 & 0 & 0 & 11.6 & 0 & 0 \\ -4.4 & -4.4 & 18.6 & 0 & 0 & 0 & 0 \end{bmatrix} \frac{\text{C}}{\text{m}^2} \quad \mathbf{e}_h = \begin{bmatrix} 0 & 0 & 0 & 0 & 0 & 5.5 \\ 0 & 0 & 0 & 0 & 5.5 & 0 \\ 5.8 & 5.8 & 7 & 0 & 0 & 0 \end{bmatrix} \text{T} \quad (58)$$

$$\mathbf{C} = \begin{bmatrix} 116 & 77 & 78 & 0 & 0 & 0 \\ 77 & 116 & 78 & 0 & 0 & 0 \\ 78 & 78 & 162 & 0 & 0 & 0 \\ 0 & 0 & 0 & 89 & 0 & 0 \\ 0 & 0 & 0 & 0 & 86 & 0 \\ 0 & 0 & 0 & 0 & 0 & 86 \end{bmatrix} \text{GPa}$$

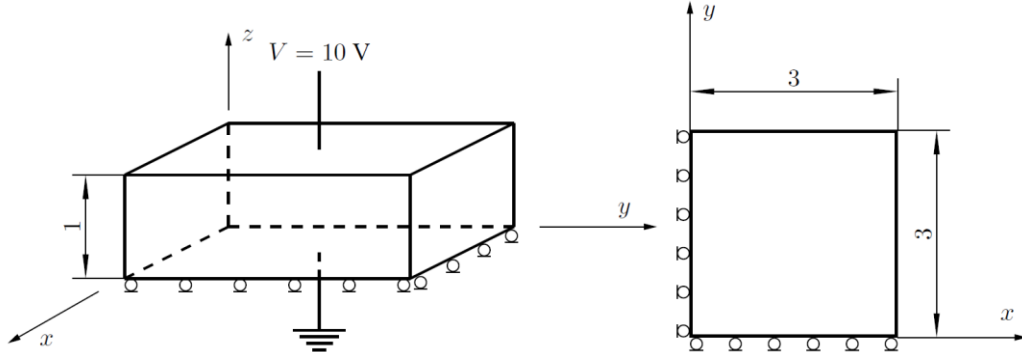


Fig. 1 Sketch of the boundary conditions considered for the actuator validation example. Three planes of symmetry considered in $x = y = z = 0$; electric potential prescriptions at the top and bottom planes. Measures in mm

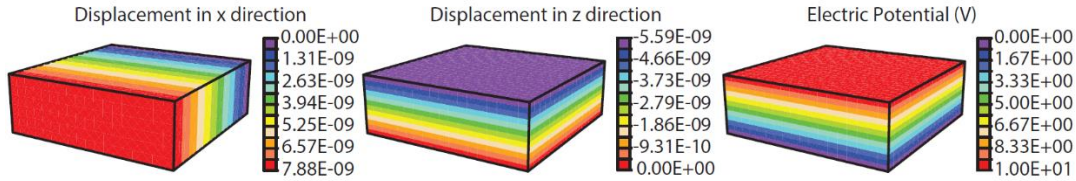


Fig. 2 Displacement in directions x and z and electric potential distributions for the actuator validation piezoelectric case

5.1 Piezoelectricity

A piezoelectric material is considered having null coefficients and tensors in (38) except for \mathbf{C} , \mathbf{e}_e and $\boldsymbol{\epsilon}$. Therefore, only electric and mechanic field variables matter in this section. This material works two ways: as actuator, which can induce movements when an electric field is applied, or as generator, for which when a displacement or a force is applied, an electric potential distribution is generated.

In Fig. 1, the boundary conditions for the first validation example can be seen with the piezoelectric working as actuator. Regarding the mechanic field, symmetry conditions have been taken into account so that an eighth of a simple box geometry with dimensions $6 \times 6 \times 2$ mm is represented. As for the electric field, $V = 10$ V at the top and ground at the z symmetry plane have been set.

The voltage difference between the top and the bottom faces is generating a component of \mathbf{E} in direction z while the others remain zero. The piezoelectric coefficient couples the electric with the mechanic field generating displacements. Since the z direction is the polarized, the induced displacements in all directions are proportional to coefficients $e_{e,31}$, $e_{e,32}$ and $e_{e,33}$ respectively. As the boundary conditions do not prevent these movements, no stresses appear and the equality $\mathbf{C}\boldsymbol{\epsilon} = \mathbf{e}_e\mathbf{E}$ holds.

The appearance of strains modifies the electric displacement \mathbf{D} field. However, no change is expected in \mathbf{E} since the electric potential is not affected by the coupling in this particular example. In Fig. 2, a summary of all relevant distributions calculated by FEAP is shown; these distributions are linear as expected. All displacements are proportional to the piezoelectric coefficients

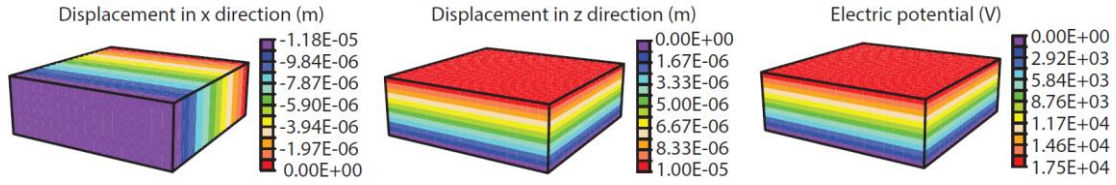


Fig. 3 Displacement in directions x and z and electric potential distributions for the generator validation piezoelectric case

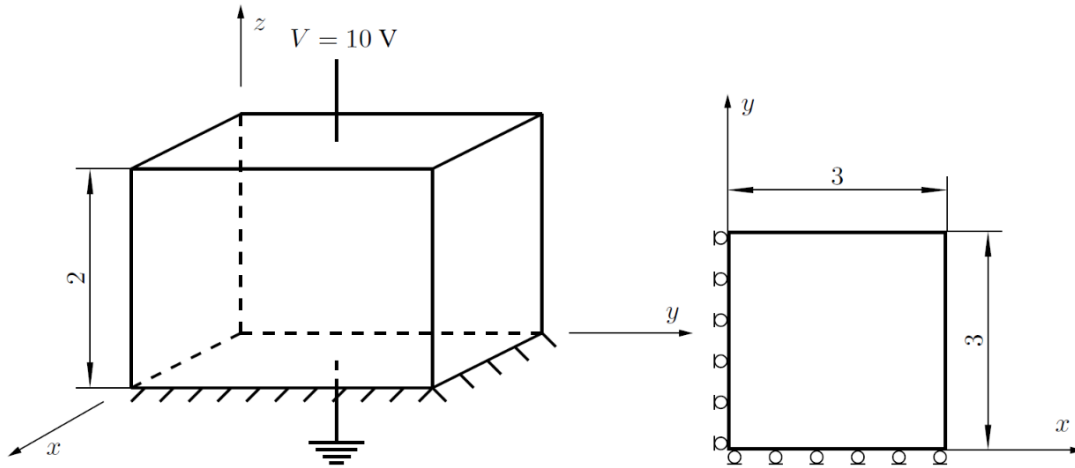


Fig. 4 Sketch of the boundary conditions considered for the third piezoelectric example. Two planes of symmetry considered in $x = y = 0$; electric potential prescriptions at the top and bottom planes; the latter face clamped. Measures in mm

mentioned before (y direction distribution not displayed but equal to the one of x). Note that u_z is negative while u_x and u_y are positive, due to the numerical values assigned to $e_{e,31}$ and $e_{e,32}$. The also linear V cause a constant distribution of E_z , not shown in the figure for simplicity.

The complementary case, for which the piezoelectric material is used as generator is also run for another validation. The problem is set with the same boundary conditions as in Fig. 1, but instead of $V = 10$ V, a vertical uniform displacement of a hundredth of the z length is prescribed at the top.

The displacement u_z is linear due to the applied prescription (see Fig. 3), while u_x appears because of the crossed coefficients C_{13} and C_{23} being negative due to the Poisson ratio. The piezoelectric coupling generates a linear V distribution and therefore a constant E_z . Analogously to the previous example, the boundary conditions enforce a zero \mathbf{D} , therefore $\mathbf{e}_e \boldsymbol{\varepsilon} = -\boldsymbol{\varepsilon} \mathbf{E}$.

Another example, not so straightforward, is run under the boundary conditions prescribed of Fig. 4. This time a quarter of the box is being modeled, due to the non-symmetric mechanic boundary conditions: at the bottom, all the degrees of freedom, including the electric potential, are set to zero. The other boundary conditions remain equal, that is, with symmetry in planes $x = y = 0$ and voltage of 10 V at the top.

In this case, the plane $z = 0$ is clamped, concentrating all stresses there as can be seen in Fig. 5. Both u_x and u_y displacements are skewed due to the boundary conditions. To fully appreciate the movement, the deformed configuration is also given.

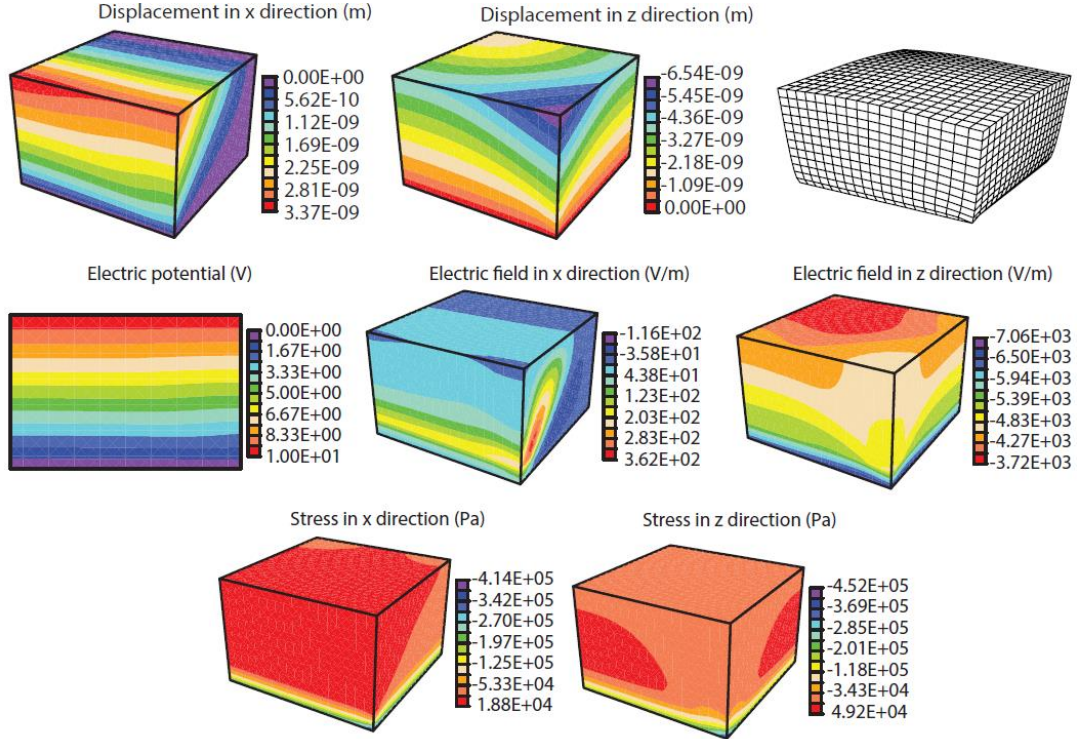


Fig. 5 Displacement in directions x and z , deformed configuration amplified 10^5 , electric potential, electric field and stresses in directions x and z distributions for piezoelectric clamped case

The electric potential may seem linear, but it can be appreciated in the figure that near the bottom the isolines are closer among themselves than at the top; near the right free edge the isolines are also closer and not straight. Hence, the E_z component is not constant and for E_x some concentrations appear near the lower frontal edge (the distribution for E_y is the same). The value of the latter is an order of magnitude lower than the former.

5.2 Piezo-electro-magnetism

First, a simple piezomagnetic case with the same configurations as before is studied; the only non-zero tensors are \mathbf{C} , \mathbf{e}_h and $\boldsymbol{\mu}$. Instead of electric potential for the boundary conditions, magnetic potential is applied. The obtained results give similar values to the previous ones, but with different numbers due to the difference in \mathbf{e}_h and $\boldsymbol{\mu}$ with respect to \mathbf{e}_c and $\boldsymbol{\epsilon}$. This coincidence is due to the similarities between the electric and magnetic field.

A more complex piezo-electro-magnetic material is simulated; therefore, all the previous piezoelectricity and piezomagnetism tensors and also \mathbf{v} are active now. With this hypothetical material, the same example as in Fig. 4 but with $\varphi = 10$ C/m at the top and $\varphi = 0$ C/m at the bottom is run.

In Fig. 6, a mosaic with the most important magnitudes calculated by FEAP can be seen. The displacements come from the superposition of electric and magnetic fields; for instance, the electric field generates positive u_x while the magnetic field induces negative ones. Since $e_{h,31}$ is

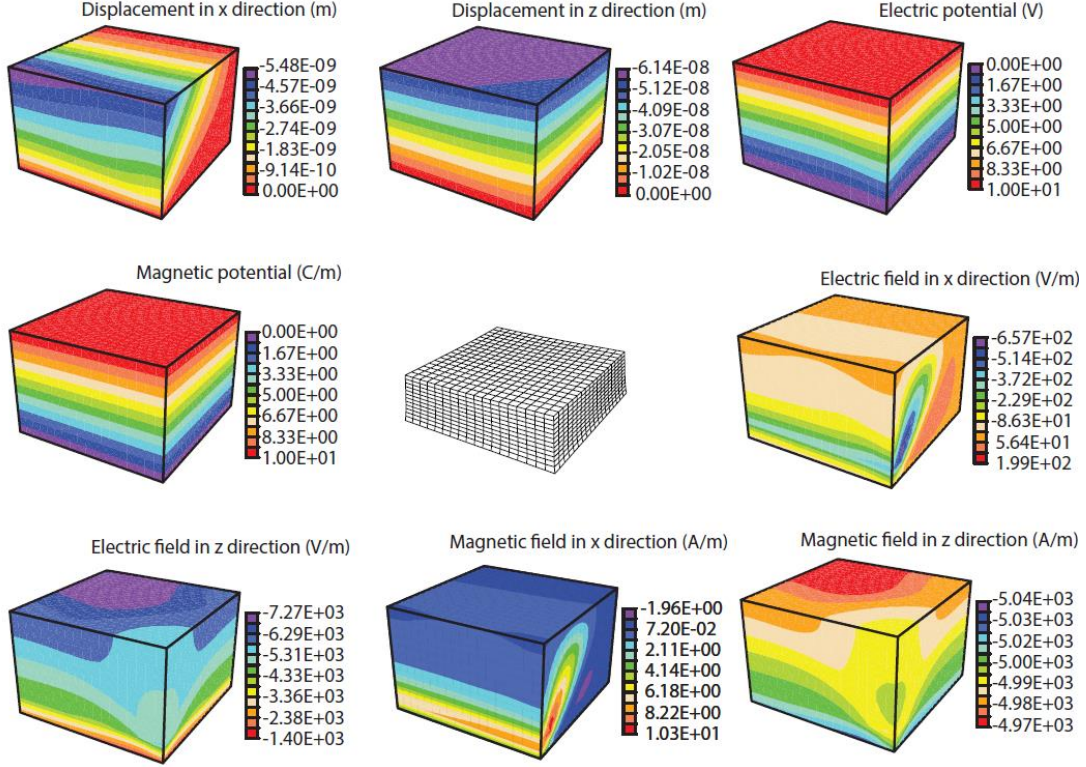


Fig. 6 Displacement in directions x and z , electric potential, magnetic potential, deformed configuration amplified 10^5 , electric and magnetic fields in directions x and z distributions for piezo-electro-magnetic clamped case

higher than $e_{e,31}$, the sum of both displacements is a negative one. Otherwise, both fields generate negative displacements for u_z , so that all contribute are in the same direction. The deformed configuration amplified by 2×10^4 times, and it is given in the central figure for better understanding of the displacements.

As for the electric and magnetic fields, their distributions are basically the same: for E_x and H_x a concentration appears near the bottom front edge due to the boundary conditions, and for E_z and H_z the concentration is near the bottom plane; in the free edge a homogeneous distribution can be seen. The higher value of μ with respect to ϵ is what causes the almost insignificant variation of H_z and a negligible H_x . For the electric field, E_x is only one order of magnitude lower than E_z . Since \mathbf{H} is the predominant field, the u_z distribution is more regular than the one displayed in Fig. 5.

5.3 Thermoelasticity

For the thermoelastic behavior the only tensors or coefficients not null from the constitutive (38) are β , \mathbf{C} and $\rho_m c_v$. A first benchmark example is calculated under the same geometry and mechanical boundary conditions as in Fig. 1. Temperature boundary conditions are required instead of the electric ones: the value for T at the top and the bottom is $T_0 + 20$ K and the other faces have adiabatic boundary conditions.

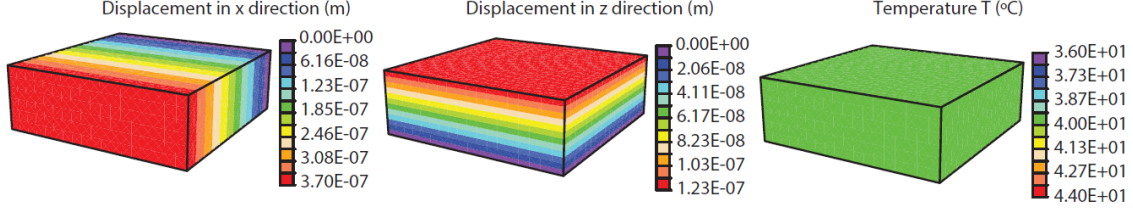
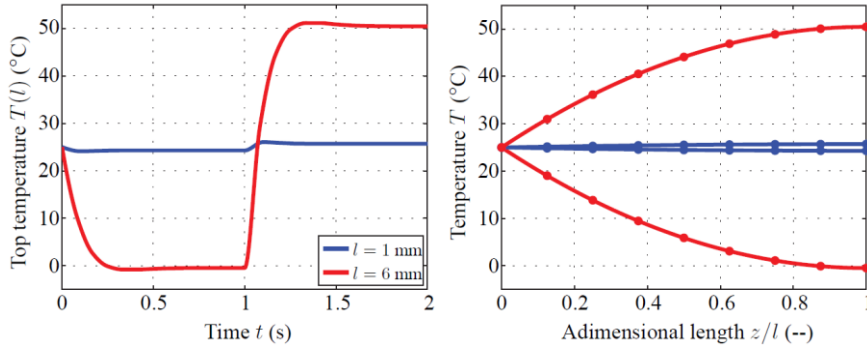

 Fig. 7 Displacement in directions x and z and temperature distributions for the thermoelastic validation case


Fig. 8 Left, transient temperature distribution at the top of the geometry of a thermoelastic case; right, temperature distribution along the vertical direction for time slightly lower than 1 and 2 s

This example is run in FEAP for static case obtaining the results in Fig. 7. Since T is both a degree of freedom and a dual variable, the regular benchmark result could only be obtained with constant temperature. In this case, a linear distribution for all displacements is obtained and the distributions are the same as expected from analytical results. All displacements are positive since T is greater than the reference temperature. Despite the fact that the expansion coefficient is isotropic, β is not due to the elasticity tensor \mathbf{C} .

An opposite benchmark result could be obtained imposing a constant and homogeneous value for $\dot{\epsilon} = 0.01$ and keeping only the boundary for $T = T_0$ at the bottom, imposing the adiabatic condition also at the top side so that the temperature can change. The imposed displacement is introduced at the top first with an increasing ramp until $t = 1$ s and then returning to zero with the same pace until $t = 2$ s; the movement at the bottom is restrained.

In Fig. 8 left the transient distributions of T on the top surface are plot for two different heights measured along the coordinate z . When $\dot{\epsilon}$ is positive T significantly decreases up to 0.25 s and after remains constant until the ramp sign is changed, stabilizing the temperature in a steady-state that can be calculated analytically. When $\dot{\epsilon}$ is negative a smooth transition to a T symmetric increase is observed. The effect is much less pronounced when the height is small ($l = 1$ mm), since it is analytically demonstrated that it depends on l^2 .

This analytic solution is obtained solving an easier version of the heat equation with constant $\dot{\epsilon}$, assuming that Poisson modulus is null and unidimensionality. The temperature expression derived is

$$T(z) = \frac{T_0 \beta_3 \dot{\epsilon}_3}{2\kappa} z(z - 2l) + T_0 \quad (59)$$

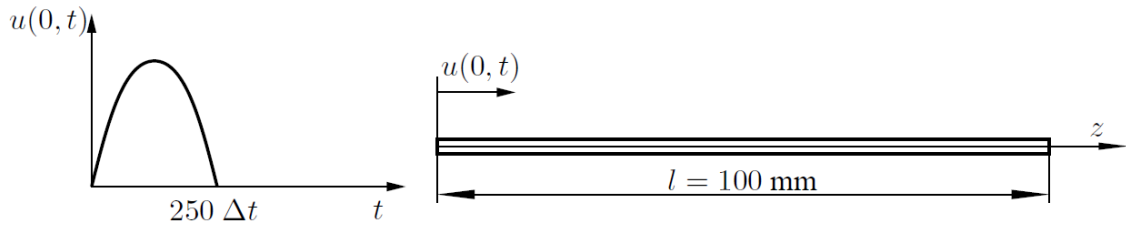


Fig. 9 Scheme of the geometry considered and the pulse applied to the left end of the bar

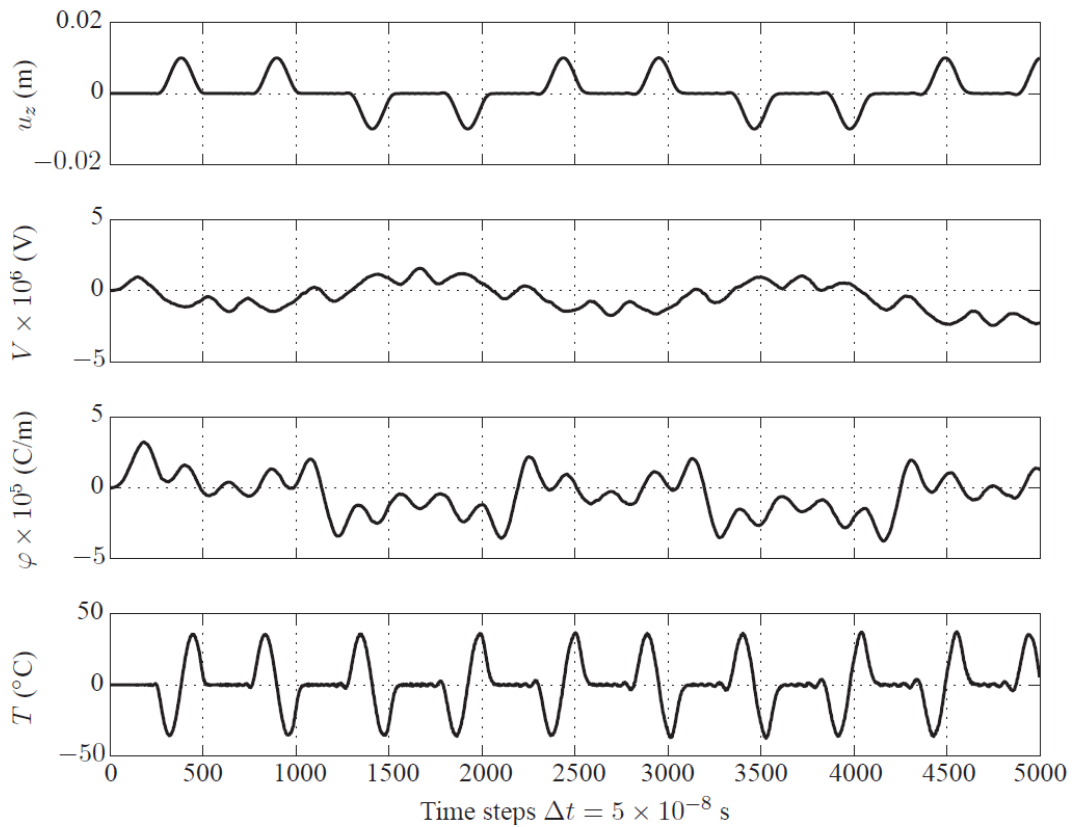


Fig. 10 Computed displacement, electric potential, magnetic potential and temperature in the bar middle point $z = l/2$

In the right figure, results for this solution (solid line) and for the numerical FEAP (circles) along the height are shown; the bottom two lines are at an instant right before 1 s, the top ones right before 2 s, all of them when T is stabilized. It is clear that this temperature varies quadratically with the height and that again the effect of the thermoelasticity coupling is much more evident for the large height.

5.4 Elastic pulse under complete coupling

In this example, we consider a transient problem for which different coupling effects can be

presented, thus providing the sort of qualitative benchmark result. Namely, we compute a thermo-electro-magneto-mechanical coupling in 3D domain in the form of a bar, with z dimension significantly larger than the other two ($1 \times 1 \times 100$ mm); this dimension is chosen for preferential polarization and magnetization. The boundary conditions are chosen taking into account the propagation to be studied along the bar: a displacement varying in time is imposed at the bar left end, while the right end is free. We also impose adiabatic boundaries for the thermal and isolated contours for the electromagnetic fields (see Fig. 9). The choice of Newmark scheme parameters $\gamma = 0.5$ and $\beta = 0.25$ is in agreement with the trapezoidal second order scheme.

The bar is set in motion by a sinusoidal displacement pulse imposed on the left end of maximum amplitude $u_z = 10$ mm; this pulse propagates through the bar, with a period much lower than that of the bar. This displacement produces the corresponding local change in strain and in its time derivative, which further generates the couplings in (38).

In Fig. 10 we present the computed response for the displacement in the longitudinal direction of the bar, for the electric potential, for the magnetic potential and for the temperature in the middle $z = l/2$, through the transient sequence. The time scale used for all of them is the step size $\Delta t = 5 \times 10^{-8}$ s.

Regarding the evolution of the mechanical field (first figure), this problem can be examined as a wave propagation: when the wave arrives to the right end, the reflected wave keeps the same sign due to the free end of the bar. However, when the reflected wave arrives to the left, the sign changes due to the built-in boundary. Since there is no dissipation implemented in the formulation, the wave conserves its maximum value and its period along the simulation.

This displacement wave creates perturbations in the other dual variables through the tensors \mathbf{e}_e , \mathbf{e}_h and $\boldsymbol{\beta}$, creating variations in the other degrees of freedom.

The temperature is analyzed first; this degree of freedom is proportional to the strain rate and also depends on the direction of the wave through (40). Thus, when a wave of positive displacement comes from the left to the right (inducing a positive heat gradient), T experiences first a decrease and second an increase, driven by first a negative strain rate and second a positive one in the same wave. After the wave bounces off the free end, the heat gradient is now negative, then T first increases and second decreases. The contrary happens when the displacement wave is negative.

As for the electric and magnetic fields, their response cannot be interpreted directly since the absence of essential boundary conditions prevents the uniqueness of the solution. In Fig. 11, the waves in a contour plot from FEAP for both V and φ can be appreciated. The images are taken at the instant when the maximum value of u_z is at the bar middle. The shape of both waves is equal to that of the elastic field, but the zones outside this wave influence have values different than zero.

6. Conclusions

In this paper, several novelties have been implemented for linear elastic mechanical system coupled with thermo-electro-magnetic in dielectrics. In particular, a complete formulation is developed in a consistent manner by using conservation principles along with the quadratic form of the free-energy potential, providing a hyperelastic response (rather than a hypoelastic) with the full coupling between all state variables and their duals. The proposed coupling results in the corresponding linear constitutive expressions for this kind of behavior. However, this still allows for nonlinear evolution of other field variables.

The formulation has been implemented in a 3D framework by using 8-node hexahedral finite elements, as the first basic equal-order discrete approximation. The time integration is performed by using the second order Newmark scheme with the optimal choice of the parameters. The nonlinear part of the system is handled by Newton-Raphson iterative scheme.

The main novelty of such a comprehensive formulation is in providing the basis for the analysis of practical cases going beyond the classical ones such as piezoelectric, thermoelastic or magnetostrictive towards more complex combinations of the coupled fields. The chosen numerical simulations have tested the model capabilities to represent for piezoelectric and piezomagnetic static cases, as well as their combination. The results illustrate the wealth of coupled responses simulations, including the transient fully-coupled pulse propagation in 3D setting.

Acknowledgments

This work was supported jointly by Hauts-de-France Region (CR Picardie) (120-2015-RDISTRUCT-000010 and RDISTRUCT-000010) and EU funding (FEDER) for Chaire-de-Mécanique (120-2015-RDISTRUCTF-000010 and RDISTRUCTI-000004). Also, by the grant Ministerio de Educación, Cultura y Deporte PRX16/00501. This support is gratefully acknowledged.

References

- Aboudi, J. (2001), "Micromechanical analysis of fully coupled electro-magneto-thermo-elastic multiphase composites", *Smart Mater. Struct.*, **10**(5), 867.
- Allik, H. and Hughes, T. (1970), "Finite element method for piezoelectric vibration", *J. Numer. Meth. Eng.*, **2**(2), 151-157.
- Babuska, I., Szabo, B.A. and Katz, I. (1981), "The p-version of the finite element method", *SIAM J. Numer. Anal.*, **18**(3), 515-545.
- Balanis, C. (1989), *Advanced Engineering Electromagnetics*, John Wiley & Sons.
- Chen, W., Lee, K. and Ding, H. (2004), "General solution for transversely isotropic magneto-electro-thermoelasticity and the potential theory method", *J. Eng. Sci.*, **42**(13), 1361-1379.
- De Groot, S. and Mazur, P. (1984), *Non-Equilibrium Thermodynamics*, Dover.
- Duczek, S. and Gabbert, U. (2013), "Anisotropic hierarchic finite elements for the simulation of piezoelectric smart structures", *Eng. Comput.*, **30**(5), 682-706.
- Ferrari, A. and Mittica, A. (2013), "Thermodynamic formulation of the constitutive equations for solids and fluids", *Energy Convers. Manage.*, **66**, 77-86.
- Fung, R.F., Huang, J.S. and Jan, S.C. (2000), "Dynamic analysis of a piezothermoelastic resonator with various shapes", *J. Vibr. Acoust.*, **122**(3), 244-253.
- Görnandt, A. and Gabbert, U. (2002), "Finite element analysis of thermopiezoelectric smart structures", *Acta Mech.*, **154**(1), 129-140.
- Hou, P., Ding, H. and Leung, A. (2006), "The transient responses of a special non-homogeneous magneto-electro-elastic hollow cylinder for axisymmetric plane strain problem", *J. Sound Vibr.*, **291**(1), 19-47.
- Ibrahimbegovic, A. (2009), *Nonlinear Solid Mechanics: Theoretical Formulations and Finite Element Solution Methods*, Springer Science & Business Media.
- Jiang, J.P. and Li, D.X. (2007), "A new finite element model for piezothermoelastic composite beam", *J. Sound Vibr.*, **306**(3), 849-864.

- Lezgy-Nazargah, M., Vidal, P. and Polit, O. (2013), "An efficient finite element model for static and dynamic analyses of functionally graded piezoelectric beams", *Compos. Struct.*, **104**, 71-84.
- Li, J. (2000), "Magnetoelastoelectroelastic multi-inclusion and inhomogeneity problems and their applications in composite materials", *J. Eng. Sci.*, **38**(18), 1993-2011.
- Moreno-Navarro, P., Ibrahimbegovic, A. and Pérez-Aparicio, J. (2017), "Plasticity coupled with thermo-electric fields: Thermodynamics framework and finite element method computations", *Comput. Meth. Appl. Mech. Eng.*, **315**, 50-72.
- Pan, E. (2001), "Exact solution for simply supported and multilayered magneto-electro-elastic plates", *J. Appl. Mech.*, **68**(4), 608-618.
- Pérez-Aparicio, J.L., Palma, R. and Taylor, R.L. (2016), "Multiphysics and thermodynamic formulations for equilibrium and non-equilibrium interactions: Non-linear finite elements applied to multi-coupled active materials", *Archiv. Comput. Meth. Eng.*, **23**(3), 535-583.
- Ramirez, F., Heyliger, P.R. and Pan, E. (2006), "Free vibration response of two-dimensional magneto-electroelastic laminated plates", *J. Sound Vibr.*, **292**(3), 626-644.
- Rao, S. and Sunar, M. (1993), "Analysis of distributed thermopiezoelectric sensors and actuators in advanced intelligent structures", *AIAA J.*, **31**(7), 1280-1286.
- Ryu, J., Carazo, A., Uchino, K. and Kim, H. (2001), "Magnetolectric properties in piezoelectric and magnetostrictive laminate composites", *Jap. J. Appl. Phys.*, **40**(8R), 4948.
- Safari, A. and Akdogan, E. (2008), *Piezoelectric and Acoustic Materials for Transducer Applications*, Springer Science & Business Media.
- Smith, R. (2005), *Smart Material Systems: Model Development*, Siam.
- Wang, X. and Zhong, Z. (2003), "A finitely long circular cylindrical shell of piezoelectric/piezomagnetic composite under pressuring and temperature change", *J. Eng. Sci.*, **41**(20), 2429-2445.
- Zienkiewicz, O. and Taylor, R. (2005), *The Finite Element Method*, Elsevier.